ISSN 1392–1320 MATERIALS SCIENCE (MEDŽIAGOTYRA). Vol. 28, No. 3. 2022

Corrosion Behavior of Spherical Chromium Carbide Reinforced NiCrBSi Hardmetal Coatings in Sulphuric Acid Solution

Li FAN [1], Xue-ying LI [2]*, Hai-yan CHEN [3], Hai-liang DU [1], Lei SHI [1]

[1] *College of Mechanical and Electronic Engineering, Shanghai Jian Qiao University, Shanghai 201306, China*
[2] *College of Information Technology, Shanghai Ocean University, Shanghai 201306, China*
[3] *College of Ocean Science and Engineering, Shanghai Maritime University, Shanghai 201306, China*

crossref http://dx.doi.org/10.5755/j02.ms.29584

Received 10 August 2021; accepted 02 December 2021

In the present work, four groups of spherical chromium carbide reinforced NiCrBSi hardmetal coatings were prepared on AISI 4145 steel by plasma transferred arc (PTA) technique. The corrosion behavior of the four as-received hardmetal coatings in 0.5 mol/L H_2SO_4 solution was investigated by polarization curve and electrochemical impedance spectroscopy (EIS). The results revealed that more Cr-rich carbides (Cr_3C_2, Cr_7C_3 and $M_{23}(C, B)_6$) are formed in the chromium carbide reinforced coatings, while for the NiCrBSi hardmetal coating only Cr_7C_3 carbide was detected by XRD. The polarization results show that the chromium carbide reinforced NiCrBSi hardmetal coatings have positive corrosion potential and lower corrosion current, providing a better protective effect to the substrate metal. The combined effects of Cr-rich carbide ceramic phases and a more stable passive film of Cr_2O_3 greatly improved the corrosion resistances of the chromium carbide reinforced NiCrBSi hardmetal coatings. The coating with the highest spherical chromium carbide addition has more pores because of the thermal stress due to the difference of thermal expansion coefficient between the NiCrBSi bonding phase and chromium carbide reinforced phase. The negative effects of the pores weaken the corrosion resistance, and the coating with the 30% chromium carbide content shows the best corrosion resistance. For NiCrBSi hardmetal coatings with higher reinforced chromium carbide content, the repeatability of the corrosion current obtained by polarization fitting is not as good as that of coatings with lower chromium carbide content. The repeatability of polarization results becomes worse when the specimens keep in a more stable passive state.

Keywords: NiCrBSi alloy, spherical chromium carbide, corrosion resistance, electrochemical techniques.

1. INTRODUCTION

AISI 4145 medium carbon alloy steel is widely used in offshore oil drilling and recovery equipment [1]. In general, due to the harsh working conditions, the surfaces of these components are subjected to serious wear and corrosion or even erosive-corrosive wear. Wear and corrosion have drastically reduced their reliable operation and service life. In general, the depositions of surface protective coatings on the metal substrate are very promising alternatives to increase the wear and corrosion resistance of these components [2, 3].

Ceramic particle reinforced metal matrix composite (MMC) coatings are generally known for their superior performances under aggressive environments, such as high wear and corrosion resistance [4, 5]. The metal matrix binder provides the composite hardmetal coatings with excellent ductility and toughness, while the reinforced ceramic particle provides the coatings with high hardness and wear resistance. These features make ceramic particle reinforced MMC coatings attractive in the petrochemical applications.

In the ceramic particle reinforced MMCs, the metal matrix can be Co-based, Ni-based or Fe-based alloys acting as the bonding phases. NiCrBSi self-fluxing alloy is a typical representative of Ni-based alloy, possessing high hardness, excellent wear resistance, and corrosion resistance. NiCrBSi plasma surfacing alloy coating is mainly composed of Ni-based solid solution (γ-Ni), carbide (M_7C_3), and boride (Ni_2B, CrB) [6]. Chen et al. [7] studied the microstructure of Ni50 coating and found that it was mainly composed of γ-(Ni, Fe) eutectic phase, carbide (Cr_7C_3, Cr_3C_2, $M_{23}C_6$), and low melting point eutectic phase (Ni_3B, Ni_3Si). Compared with the steel substrate, the wear resistance is greatly improved. The properties of NiCrBSi alloy are determined by its chemical composition. The addition of B and Si elements lowers the melting points of NiCrBSi alloys. While Cr can form hard phases such as chromium carbide or chromium boride, so the wear resistance of the NiCrBSi coating is enhanced. Also, previous researches have revealed that the NiCrBSi coatings exhibited excellent corrosion resistance with higher Cr content [8, 9].

The reinforcement mainly consists of carbide, boride, nitride, oxide, and other ceramic particles. As compared with other ceramic particles, such as tungsten carbide (WC) and titanium carbide (TiC), chromium carbide (Cr_3C_2) has the following characteristics [10 – 12]: closer density to that of Ni-based alloy, and smaller difference of the thermal expansion coefficient between Cr_3C_2 (10.3×10^{-6}/°C) and NiCrBSi alloy (11.4×10^{-6}/°C).

Previous studies compared the corrosion behaviors of NiCrBSi alloy coating in 3.5 wt.% NaCl solution, 1mol/L NaOH, 0.5 mol/L H_2SO_4, and 0.5 mol/L HCl, and found that the NiCrBSi alloy was highly resistant to corrosion in the 1 mol/L NaOH solution [13]. While the

*Corresponding author. Tel: +86-02138122029;
E-mail address: *xyli@shou.edu.cn* (X. Li)

corrosion results in the 3.5 wt.% NaCl solution, 0.5 mol/L H_2SO_4, and 0.5 mol/L HCl shown that is Cl^- more corrosive for the NiCrBSi alloy coating than SO_4^{2-}. Cho et al. [8] studied the corrosion behaviors of four thermal sprayed WC cermet coatings with different metallic binders in 5 wt.% H_2SO_4 solution. The results revealed that the coatings containing Cr were more resistant to H_2SO_4 solution corrosion than the coating without Cr. The formation of Cr passive film suppressed the dissolution of binder metal elements. The addition of Cr enhanced the corrosion resistance in weak acidic and saline solutions [14, 15].

However little information is now available on the corrosion behaviors of plasma transferred arc deposited NiCrBSi-Cr_3C_2 ceramic coating in sulphuric acid solution, especially a special focus on different spherical Cr_3C_2 addition. Thus, for further application of the NiCrBSi-Cr_3C_2 ceramic coatings, the corrosion behaviors of such developed coatings in sulphuric acid solution or other corrosive mediums should be extensively investigated.

In this paper, four groups of spherical Cr_3C_2 reinforced NiCrBSi hardmetal coatings with different Cr_3C_2 content were deposited by PTA surfacing. The corrosion behavior of so developed spherical Cr_3C_2 reinforced NiCrBSi hardmetal coatings were studied by means of electrochemical tests in the 0.5 mol/L H_2SO_4 solution. The present research is aiming to provide a systematic evaluation of the corrosion resistance of spherical Cr_3C_2 reinforced NiCrBSi hardmetal coatings in sulphuric acid solution, paying a special focus on the effect of different Cr_3C_2 content. This study can provide experimental data for further application of such a developed Cr_3C_2 reinforced NiCrBSi hardmetal coating in an acidic environment.

2. EXPERIMENTAL SECTION

2.1. Materials

In the present study, 100 mm × 100 mm × 10 mm AISI 4145 steel (chemical composition, in weight %: C 0.45, Si 0.35, Cr 1.15, Mo 0.20, Mn 0.90, Fe balance) was utilized as the substrate. Before the PTA welding, one face of the AISI 4145 substrate steel was sandblasted and acetone-cleaned.

Two commercial powders were selected in this experiment. One is Cr_3C_2 powder with irregular shape (as shown in Fig. 1), and the other is spherical NiCrBSi powder (as shown in Fig. 2 a), compositions of these two powders are summarized in Table 1. The particle size of the chosen NiCrBSi powder was 45 – 225 μm (as shown in Fig. 2 b) in a Gauss distribution. The average particle size is about 115 μm, which is suitable for surfacing welding [16].

Table 1. Composition of the NiCrBSi and Cr_3C_2 powders

Materials	Chemical composition, wt.%
NiCrBSi	Fe 3.7, Cr 14.8, C 0.75, B 3.1, Si 4.3 Ni balance
Cr_3C_2 powder	C 12.9, O 0.5, Fe 0.2, Cr balance

2.2. Spheroidization of Cr_3C_2 particles

When used in surfacing coating, irregular powders are easy to cause stress concentration and cracks under load, thus leading to performance defects of the PTA coating. While, spherical particles can effectively reduce the cohesion and friction between the powder particles, enhance the fluidity of the powder, and further improve the quality of the coating.

In the present study, a spheroidization experiment of the irregular Cr_3C_2 particles was performed on the Tekna SY-110 induction plasma equipment (Tekna Company, Canada) under optimized process parameters (as shown in Table 2) after several experiments.

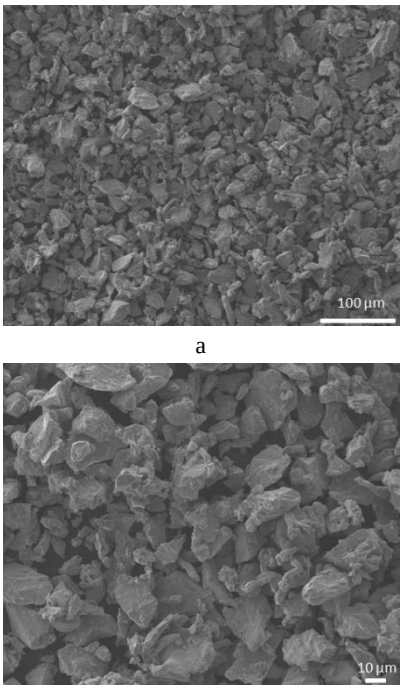

Fig. 1. SEM morphology of the original Cr_3C_2 powder: a – low magnification; b – high magnification

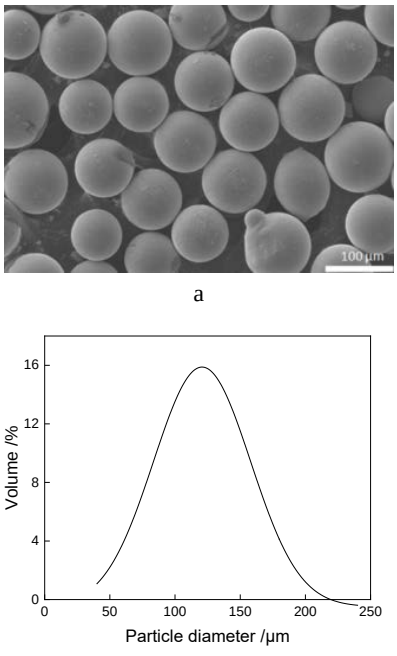

Fig. 2. a – SEM morphology of NiCrBSi powder; b – particle size distribution of NiCrBSi powder

The SEM morphology of the spheroidized Cr_3C_2 is shown in Fig. 3. From Fig. 3 it can be seen that the prepared spherical Cr_3C_2 particle has a standard spherical structure, the surface is smooth and is well dispersed.

Table 2. Parameters of induction plasma spheroidization process

Parameters	Set value
Feed rate	110 g/min
Carrier gas (Ar)	5 L/min
Flow rate of working gas	80 L/min
Flow rate of auxiliary gas (H_2)	35 L/min
Sheath gas (Ar)	25 L/min
Pressure	0.1 MPa
Power	50 kW

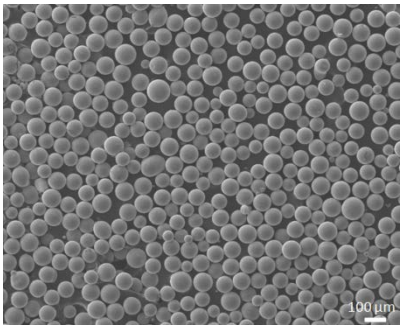

a

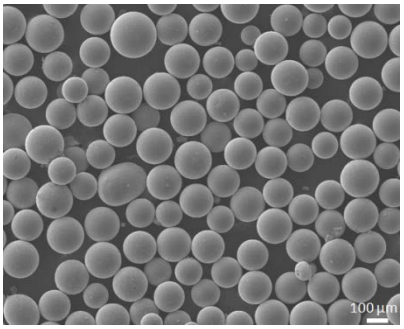

b

Fig. 3. SEM morphology of the spherical Cr_3C_2 powder: a – low magnification; b – high magnification

XRD pattern and particle size distribution of the prepared spherical Cr_3C_2 powder are shown in Fig. 4. It can be seen that the phases of spherical Cr_3C_2 powder are mainly composed of Cr_3C_2 and some free state C. The particle size is 50 – 250 μm, and the average particle size is 135 μm.

2.3. Fabrication of the coatings

The reinforced spherical Cr_3C_2 powder and NiCrBSi powder were mixed with the proportion described in Table 3.

Table 3. Composition ratio of composite powders

Specimen number	NiCrBSi content, wt.%	Cr_3C_2 content, wt.%
0#	100	0
10#	90	10
30#	70	30
50#	50	50

Then, the mixed powders were put into a QM-3SP4 planetary ball mill for 2 h and baked at 150 ℃ in the oven for 30 min to eliminate the moisture. A PTA-400E4-LM plasma transfer arc surfacing machine was used, detailed working parameters as shown in Table 4 were optimized after several experiments. After the PTA process, the 10 mm × 10 mm× 8 mm coated samples were obtained by Wirecut Electrical Discharge Machining (WEDM) for electrochemical tests.

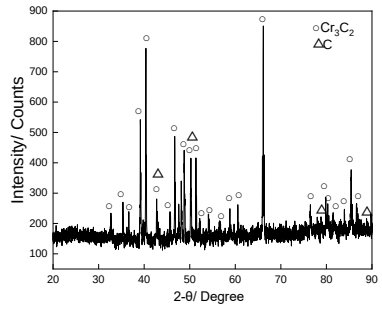

a

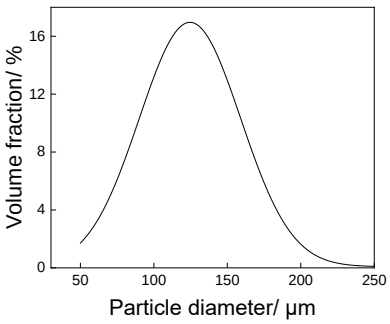

b

Fig. 4. a – XRD pattern of spherical Cr_3C_2 powder; b – particle size distribution of spherical Cr_3C_2 powder

Table 4. Working parameters for preparing PTA coatings

Parameters	Description
Current	150 A
Voltage	40 V
Feed rate	8 g/min
Speed	45 mm/min
Vibration extent	20 mm

2.4. Characterization of the coatings

The cross-section of the specimens for SEM characterization was wet ground step by step with SiC sandpaper up to 2000 grit, then polished to the mirror using 1.5 μm Al_2O_3. The bonding between the substrate and the coating and the microstructure of the coatings were analyzed by a JSM 7500F SEM (JEOL, Japan). Phase identifications of the as-received coatings were evaluated on an X-ray diffractometer (X'Pert PRO, PANalytical, Netherlands) with Cu-Kα radiation. XRD spectrums were acquired with 2θ in the range of 20° to 100° at a scan rate of 2 °/min, using 40 kV voltage and 40 mA current.

2.5. Electrochemical corrosion tests

Electrochemical corrosion tests of the four groups of Cr_3C_2 reinforced NiCrBSi hardmetal coated samples were carried out on a PGSTAT302N Autolab electrochemical workstation. The experiments were carried out three times with parallel specimens to ensure good repeatability. The 1 cm^2 effective area of the working electrode is retained and the non-working surfaces are sealed off with the organic

silica gel. The sealed electrodes were wet ground step by step to 1500 grit using emery paper. The standard three-electrode electrochemical system was employed in the corrosion experiment. The reference electrode utilized the saturated calomel electrode (SCE), the platinum plate and the polished coatings were acted as the auxiliary and the working electrodes respectively. The electrolyte solution was 0.5 mol/L H_2SO_4 prepared from reagent-grade concentrated sulfuric acid and deionized water.

The electrodes were initially immersed in the 0.5 mol/L H_2SO_4 solution, under an open circuit potential for 1 h for the system to stabilize. Then the potentiodynamic polarization curve tests began. The polarization curve tests were conducted at a 5 mV/s scanning rate in the scanning range of - 1.0 – 1.5 V.

0.01 – 100000 Hz frequency range is adopted in the electrochemical impedance spectroscopic (EIS) test, the load voltage is sinusoidal AC voltage, and the voltage amplitude is 10 mV. EIS data were fitted using Zsimpwin software with less than 1% error.

3. RESULTS AND DISCUSSION

3.1. Microstructure and structure of the PTA hardmetal coatings

Four PTA hardmetal coatings with different addition of Cr_3C_2 were successfully deposited, and the macroscopic morphology of the 30 % spherical Cr_3C_2 reinforced hardmetal coating (30# coating) sample is shown in Fig. 5. As can be seen from Fig.5, the surface morphology is smooth and without detectable cracks and pores, indicating that the selection of the PTA surfacing technology parameters is appropriate, thus high quality coatings can be obtained.

Fig. 5. Macroscopic morphology of the 30% spherical Cr_3C_2 reinforced coating (30# coating)

Fig. 6 presents the cross-section SEM images of the four PTA hardmetal coatings, and it can be seen that the thickness of the four coatings is approximately 1320 – 1470 μm. At higher magnification, it can be seen from Fig. 6 b, d, f, and h that there is a planar zone without obvious microstructure between the substrate steel and the coating. At the bonding interface of the coating and substrate steel, there are a large temperature gradient (G) and a small solidification rate (R), and the G/R value tends to infinity, which leads to the formation of planar crystal. This planar band signifies that the deposited coatings are well metallurgically bonded to the steel substrate [17]. Also, it can be seen from Fig. 6 b, d, f, and h that all the four coatings exhibit dense microstructures with low porosity detectable at these magnifications. For 30# coating and 50# coating with higher spherical Cr_3C_2 addition, some pores are appeared in the coating because of the thermal stress due to the difference of thermal expansion coefficient between the NiCrBSi bonding phase and Cr_3C_2 reinforced phase [12].

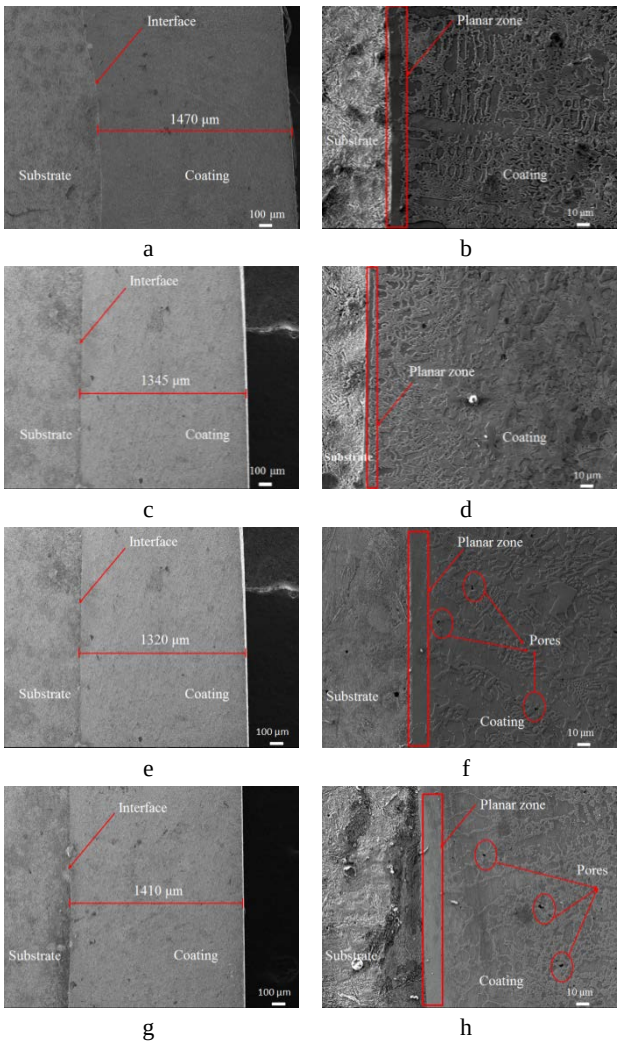

Fig. 6. Low (a, c, e, g) and high (b, d, f, h) magnified cross-sectioned SEM micrographs of four hardmetal coatings: a, b – 0# coating; c, d – 10# coating; e, f – 30# coating; g, h – 50# coating

The XRD patterns of four hardmetal coatings are given in Fig. 7.

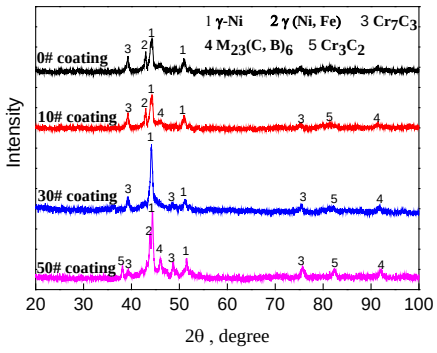

Fig. 7. XRD patterns of four as-received hardmetal coatings

It is noted that the phases of 0# coating without Cr_3C_2 addition are mainly composed of γ-Ni, γ-(Ni, Fe) and Cr_7C_3. For coatings with reinforced spherical Cr_3C_2 addition (10# coating, 30# coating, and 50# coating), the additional carbides Cr_3C_2, and $M_{23}(C, B)_6$ (M=Fe, Cr, Ni) phases are found as compared with the 0# coating. Meanwhile, the Cr_7C_3 peaks increased in number and enhanced in diffraction intensity. At high temperature, partial Cr_3C_2 particles were decomposed to Cr_7C_3 and $M_{23}(C, B)_6$ [18]. These newly formed Cr_7C_3 and $M_{23}(C, B)_6$ and the remainder incompletely melted Cr_3C_2 together guarantee the corrosion resistance of the coating.

3.2. Potentiodynamic polarization investigations

Polarization curves of four hardmetal coatings in 0.5mol/L H_2SO_4 solution are given in Fig. 8. The repeatability and repeatability of the polarization results were expressed in Standard error (ε), and the value of was calculated according to the following equation [15]:

$$\varepsilon = \sqrt{\frac{\sum_{i=1}^{N}(x_i - \bar{x})}{N^2}}, \quad (1)$$

where N is the number of tested times, in this work experiment was carried out three times so the value of N is 3. x_i is the i_{corr} value calculated by the Stern-Geary equation, and $\bar{x}$ is the mean value of i_{corr}.

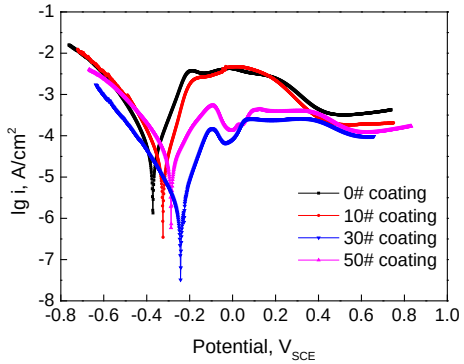

Fig. 8. Polarization curves of four hardmetal coatings in 0.5 mol/L H_2SO_4 solution

As can be seen in Fig. 8, for 0# coating and 10# coating the corrosion currents in the anodic reaction region presented an initial exponential increase with the increment of corrosion potential, then a decrease and finally kept constant with the further increment of corrosion potential. The initial exponential increase of the corrosion current corresponds to the active dissolution of the bonding materials. Sulfuric acid is a kind of oxidizing acid. In sulfuric acid solution, some possible oxides mostly Ni_2O_3, NiO, SiO_2, and little Cr_2O_3 can be formed on the surface of the NiCrBSi. The above oxides uniformly covered the surface of the coating, so that the corrosion current decreased and the corrosion gradually entered into a stable passive state. Therefore, the corrosion mechanism for 0# coating and 10# coating in sulfuric acid is characterized by active dissolution in the early stage, and passive film protection occurs in the later stage.

As compared with 0# coating and 10# coating, the 30# coating and 50# coating with higher Cr_3C_2 addition have two passive regions. The reason for the second passive region is that after the NiCrBSi bonding materials dissolve, the Cr-rich carbides (Cr_3C_2, Cr_7C_3, and $M_{23}(C, B)_6$) may contact with the corrosion medium, thus a passive film of Cr_2O_3 has uniformly adhered to the coating surface and the corrosion rate was slowed down to a certain extent. The passive current densities of 30# coating and 50# coating are one order of magnitude lower than those of 0# coating and 10# coating, demonstrating the protective effect of the more Cr-rich carbides and Cr_2O_3.

The E_{corr} (corrosion potential), and i_{corr} (corrosion current density) values were obtained by Tafel extrapolation method using the software of Autolab PGSTAT 302N working station. The fitting data and the standard error (ε) of i_{corr} are presented in Table 4.

Table 4. Corrosion parameters obtained from potentiodynamic polarization curves fitting

Materials	E_{corr}, mV	i_{corr}, μA.cm^{-2}		ε	$\frac{\varepsilon}{i_{corr}}$
0# coating	- 396.06	112.73 118.78 124.52	118.68	2.76	2.33 %
10# coating	- 338.14	47.45 62.13 54.69	54.76	3.46	6.32 %
30# coating	- 226.68	9.48 13.72 11.29	11.50	1.01	8.78 %
50# coating	- 273.04	14.52 18.23 20.14	17.63	1.81	10.29 %

Compared with the corrosion potential E_{corr} of 0# coating (- 396.06 mV), the E_{corr} values of three coatings with reinforced spherical Cr_3C_2 addition were - 338.14 mV, - 226.28 mV and - 273.04 mV for the 10# coating, 30# coating and 50# coating respectively, showing that the corrosion resistance of Cr_3C_2 reinforced coatings was much better than that of NiCrBSi coating without Cr_3C_2 addition. The current densities of the three Cr_3C_2 reinforced coatings were 54.76 μA/cm^2, 9.24 μA/cm^2 and 16.11 μA/cm^2, respectively. Compared with the corrosion current density of NiCrBSi coating without Cr_3C_2 addition, the current density of 30# coating with the 30% Cr_3C_2 content is only one tenth of its corrosion current, indicating the higher corrosion resistance of 30# coating. The addition of Cr_3C_2 reinforced particles is beneficial to improve the corrosion resistance of the NiCrBSi coating. However, with the increase of the mass fraction of Cr_3C_2, the defects such as pores increase (as illustrated in Fig. 3) and will have a negative impact on the corrosion resistance. Therefore, 30# coating with the 30 % Cr_3C_2 content shows the best corrosion resistance.

Generally speaking, the smaller the ratio between ε and i_{corr}, the better the repeatability of the polarization currents [15]. From Table 4, it can also be seen that the 0# coating without Cr_3C_2 addition has the lowest $\frac{\varepsilon}{i_{corr}}$ value among the four coatings, representing the best repeatability of the polarization results. This may be explained by the following that the method of obtaining i_{corr} by Tafel extrapolation method only suited for the activation controlled corrosion process [19]. As for the three Cr_3C_2 reinforced coatings,

there are Cr-rich carbides and passive film of Cr_2O_3 on the surface of these coatings and the protective effect of the passive film and the Cr-rich carbide ceramic phases make the coating surface in a more passive state. So, the following conclusions can be obtained that the repeatability of the polarization results will be greatly improved when the coating surface is kept in an active dissolution state, and reduced when the coating surface remained in a more stable passive state.

3.3. Electrochemical impedance spectroscopic investigations

Fig. 9 a presents the Nyquist plots of the four hardmetal coatings in the 0.5 mol/L H_2SO_4 solution. To better analyze the impedance data and explain the corrosion behavior of the hardmetal coatings, the equivalent circuit shown in Fig. 9 b was adopted in fitting the EIS experimental data. The Nyquist plots in Fig. 6 a have two capacitive loops, respectively a high-frequency loop and a low-frequency loop, illustrating that there should be two capacitive reactances in the electrode process. The low-frequency capacitive reactance is corresponding to the passive film, whilst the high-frequency capacitive reactance is related to the double-layer capacitance formed on the surface of the sample beneath the passive film. Fig. 6 a demonstrates that the radius of capacitive reactance arc of the 30# coating is greater than those of the other three coatings. The larger radius of the arc, the greater impedance of the specimen is [20]. Therefore, 30# coating has the highest corrosion resistance in H_2SO_4 solution.

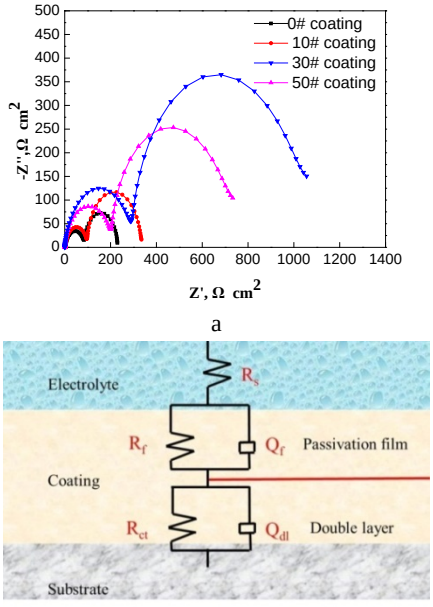

Fig. 9. a – Nyquist plots; b – equivalent circuit proposed for EIS fitting

The equivalent circuits proposed for EIS fitting are illustrated in Fig. 9 b. The validity of the fitted values was confirmed by using the K-K conversion diagram [21], as presented in Fig. 10. The good agreement of the experimental data and the fitted results, indicating that the fitting results are valid.

The EIS fitting results are presented in Table 5. Among them, R_s represents the solution resistance, Q (constant phase element, CPE) is adopted rather than capacitance, Q_f refers to the capacitance of passive film, R_f is the impedance of ions passing through passive film, R_{ct} is the electrochemical transfer resistance, Q_{dl} is used to represent the double-layer capacitance, L is inductive reactance.

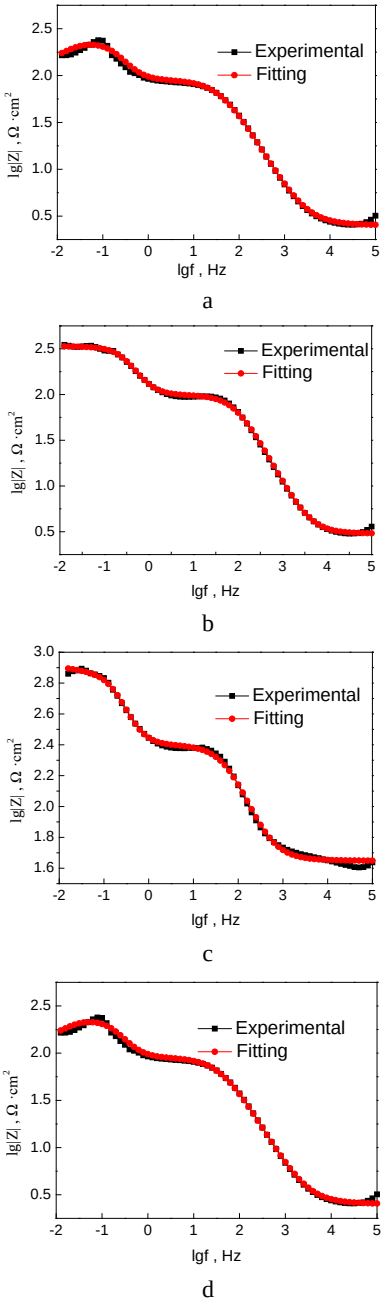

Fig. 10. K-K conversion diagram of EIS experimental data and fitting data: a – 0# coating; b – 10# coating; c – 30# coating; d – 50# coating

Parameter n in the Q indicates surface roughness and heterogeneity and the deviation from ideal dielectric behavior [22]. The Q value can be calculated by the equation:

$$Q - Y_0(j\omega)^n = Y_0\omega^n \cos\left(\frac{n\pi}{2}\right) + j\,Y_0\omega^n \sin\left(\frac{n\pi}{2}\right), \qquad (2)$$

where Y_0 is a constant directly involved with potential ($\Omega^{-1}\cdot cm^{-2}\cdot s^n$), $j^2 = -1$, ω refers to the angular frequency (rad/s), n represents a parameter without unit, its value range is $0 \le n \le 1$.

Table 5. EIS fitting results of the four as-received PTA hardmetal coatings

Samples	R_s, $\Omega \cdot cm^2$	Q_f		R_f, $\Omega \cdot cm^2$	Q_{dl}		R_{ct}, $\Omega \cdot cm^2$
		Y_0, $\Omega^{-1} \cdot cm^{-2} \cdot s^n$	n_f		Y_0, $\Omega^{-1} \cdot cm^{-2} \cdot s^n$	n_{dl}	
0# coating	3.14	6.21×10^{-7}	0.88	77.82	1.26×10^{-5}	0.91	189.65
10# coating	3.28	3.07×10^{-7}	0.96	92.54	1.54×10^{-5}	0.95	374.21
30# coating	3.84	4.27×10^{-7}	1	278.81	2.37×10^{-5}	0.99	821.68
50# coating	2.99	5.26×10^{-7}	1	324.08	2.74×10^{-5}	1	701.20

When the potential is the only variable, R_{ct} is equivalent to the polarization resistance (R_p). According to Stern-Geary equation, the corrosion current density (i_{corr}) can be calculated by the Eq. 3:

$$i_{corr} = \frac{\beta_a \beta_c}{2.303\ (\beta_a + \beta_c)} . \frac{1}{R_p} . \quad (3)$$

Table 6 shows that the R_{ct} value of coatings with reinforced spherical Cr_3C_2 addition is higher than that of NiCrBSi hardmetal coating, which is 1.97 times (10# coating), 4.33 times (30# coating) and 3.70 times (50# coating) of 0# coating. That is to say, the polarization resistance R_p values are of spherical Cr_3C_2 reinforced coatings are greater than that of NiCrBSi hardmetal coating. This is identical to the polarization curve results. The larger the R_{ct} value, the better the corrosion resistance. Therefore, the addition of reinforced Cr_3C_2 can largely improve the corrosion resistance of NiCrBSi hardmetal coating, and the coating with 30 % Cr_3C_2 addition has the best performance. Compared with 0# coating and 10# coating, there is a significant increase in R_f values for the 30# coating and 50# coating. The great increase of R_f suggests that the dissolution rate of the passive film of the 30# coating and 50# coating is smaller. It is noted that the diffusion coefficient n_f of 30# coating and 50# coating is 1, which suggests that the passive films on the 30# coating and 50# coating surface are very uniform and stable. So the passive film of 30# coating and 50# coating will have a stronger protective effect on the substrate metal.

4. CONCLUSIONS

The coatings were metallurgically bonded with the AISI 4145 steel. With the addition of Cr_3C_2 particles, more Cr-rich carbides were formed in the coatings.

The polarization results show that the Cr_3C_2 reinforced NiCrBSi hardmetal coatings have a lower corrosion current and positive corrosion potential, providing a better protective effect to the substrate metal. The combined effects of Cr-rich carbide ceramic phases and the protective passive film of Cr_2O_3 keep the Cr_3C_2 reinforced NiCrBSi hardmetal coatings in a more passive state.

The 50# coating with the highest spherical Cr_3C_2 addition has more pores because of the thermal stress due to the difference of thermal expansion coefficient between the NiCrBSi bonding phase and Cr_3C_2 reinforced phase. The negative effects of the pores weaken the corrosion resistance, and the 30# coating with the 30 % Cr_3C_2 content shows the best corrosion resistance.

For NiCrBSi hardmetal coatings with higher reinforced Cr_3C_2 content, the repeatability of the corrosion current obtained by polarization fitting is not as good as that of coatings with lower Cr_3C_2 content. The repeatability of polarization results becomes worse when the specimens keep in a more stable passive state.

Acknowledgments

This research was funded by the Science & Technology Program of Shanghai Jian Qiao University (No.SJQ19012), and Initial Scientific Research Fund of Young Teacher in Shanghai Ocean University (No.A2-2006-20-200317).

REFERENCES

1. **Liu, S.S., Chen, H.Y., Zhao, X., Fan, L., Guo, X.M., Yin, Y.S.** Corrosion Behavior of Ni-based Coating Containing Spherical Tungsten Carbides in Hydrochloric Acid Solution *Journal of Iron and Steel Research International* 26 2019: pp. 191 – 199. https://doi.org/10.1007/s42243-019-00240-y
2. **Fan, L., Chen, H.Y., Dong, Y.H., Dong, L.H., Yin, Y.S**. Wear and Corrosion Resistance of Laser-cladded Fe-based Composite Coatings on AISI 4130 steel *International Journal of Minerals Metallurgy and Materials* 25 (6) 2018: pp. 716 – 728. https://doi.org/10.1007/s12613-018-1619-2
3. **Wang, F., Zhang, F., Zheng, L., Zhang, H.** Structure and Corrosion Properties of Cr Coating Deposited on Aerospace Bearing Steel *Applied Surface Science* 423 2017: pp. 695 – 703. https://doi.org/10.1016/j.apsusc.2017.06.099
4. **Fan, L., Dong, Y.H., Chen, H.Y., Dong, L.H., Yin, Y.S.** Wear Properties of Plasma Transferred Arc Fe-based Coatings Reinforced by Spherical WC Particles *Journal of Wuhan University of Technology-Mater Science Edition* 34 (2) 2019: pp. 433 – 439. https://doi.org/10.1007/s11595-019-2070-6
5. **Xu, P., Lin, C.X., Zhou, C.Y, Yi, X.P.** Wear and Corrosion Resistance of Laser Cladding AISI 304 Stainless Steel/Al_2O_3 Composite Coatings *Surface & Coatings Technology* 238 (2) 2014: pp. 9 – 14. https://doi.org/10.1016/j.surfcoat.2013.10.028
6. **Liyanage, T., Fisher, G., Gerlich, A.P.** Influence of Alloy Chemistry on Microstructure and Properties in NiCrBSi Overlay Coatings Deposited by Plasma Transferred Arc Welding (PTAW) *Surface & Coatings Technology* 205 (3) 2010: pp. 759 – 765. https://doi.org/10.1016/j.surfcoat.2010.07.095
7. **Chen, G.Q., Fu, X.S., Wei, Y.H., Li, S., Zhou, W.L.** Microstructure and Wear Properties of Nickel-based Surfacing Deposited by Plasma Transferred Arc Welding *Surface & Coatings Technology* 228 2013: pp. S276 – S282. https://doi.org/10.1016/j.surfcoat.2012.05.125
8. **Cho, J.E., Hwang, S.Y., Kim, K.Y.** Corrosion Behavior of Thermal Sprayed WC Cermet Coatings Having Various Metallic Binders in Strong Acidic Environment *Surface and Coatings Technology* 200 (8) 2006: pp. 2653 – 2662. https://doi.org/10.1016/j.surfcoat.2004.10.142

9. **Zhao, W.M., Wang, Y., Dong, L.X., Wu, K.Y., Xue, J.** Corrosion Mechanism of NiCrBSi Coatings Deposited by HVOF *Surface & Coatings Technology* 190 (2 – 3) 2005: pp. 293 – 298. https://doi.org/10.1016/j.surfcoat.2004.04.057
10. **Ni, Z.F., Sun, Y.S., Xue, F., Bai, J., Lu, Y.J.** Microstructure and Properties of Austenitic Stainless Steel Reinforced with in situ TiC Particulate *Materials & Design* 32 (3) 2011: pp. 1462 – 1467. https://doi.org/10.1016/j.matdes.2010.08.047
11. **Fan, L., Chen, H.Y., Du, H.L., Cheng, Q., Hou, Y.** Corrosion Resistance of Nickel-Based Composite Coatings Reinforced by Spherical Tungsten Carbide *Materials Science Forum* 993 2020: pp. 1075 – 1085. https://doi.org/10.4028/www.scientific.net/MSF.993.1075
12. **Wang, J., Li, L., Tao, W.** Crack Initiation and Propagation Behavior of WC Particles Reinforced Fe-based Metal Matrix Composite Produced by Laser Melting Deposition *Optics & Laser Technology* 82 2016: pp. 170 – 182. https://doi.org/10.1016/j.optlastec.2016.03.008
13. **Chang, J.H., Chou, J.M., Hsieh, R.I., Lee, J.L.** Corrosion Behaviour of Vacuum Induction-melted Ni-based Alloy in Sulphuric Acid *Corrosion Science* 52 (7) 2010: pp. 2323 – 2330. https://doi.org/ 10.1016/j.corsci.2010.03.026
14. **Yang, X., Zhang, J., Li, G.** Cavitation Erosion Behaviour and Mechanism of HVOF-sprayed NiCrBSi-(Cr_3C_2-NiCr) Composite Coatings *Surface Engineering* 34 (3) 2018: pp. 211 – 219. https://doi.org/10.1080/02670844.2016.1258770
15. **Zhao, W.M., Wang, Y., Han, T., Wu, K.Y., Xue, J.** Electrochemical Evaluation of Corrosion Resistance of NiCrBSi coatings Deposited by HVOF *Surface & Coatings Technology* 183 (1) 2004: pp. 118 – 125. https://doi.org/10.1016/j.surfcoat.2003.09.053
16. **Saito, H., Iwabuchi, A., Shimizu, T.** Effects of Co Content and WC Grain Size on Wear of WC Cemented Carbide *Wear* 261 (2) 2006: pp. 126 – 132. https://doi.org/ 10.1016/j.wear.2005.09.034
17. **Huang, Z., Hou, Q., Wang, P.** Microstructure and Properties of Cr_3C_2-modified Nickel-based Alloy Coating Deposited by Plasma Transferred Arc Process *Surface and Coatings Technology* 202 (13) 2008: pp. 2993 – 2999. https://doi.org/10.1016/j.surfcoat.2007.10.033
18. **Kaushal, S., Gupta, D., Bhowmick, H.** On Surface Modification of Austenitic Stainless Steel using Microwave Processed Ni/Cr_3C_2 Composite Cladding *Surface Engineering* 34 2018: pp. 809 – 817. https://doi.org/ 10.1080/02670844.2017.1362808
19. **Angst, U., Büchler, M.** On the Applicability of the Stern-Geary Relationship to Determine Instantaneous Corrosion Rates in Macro-cell Corrosion *Materials & Corrosion* 66 (10) 2015: pp. 1017 – 1028. https://doi.org/10.1002/maco.201407997
20. **Dong, Y.H., Fan, L., Chen, H.Y., Dong, L.H., Yin, Y.S., Sun, F.H.** Corrosion Behavior of Plasma Transferred Arc Fe-Based Coating Reinforced by Spherical Tungsten Carbide in Hydrochloric Acid Solutions *Journal of Wuhan University of Technology-Mater Science Edition* 35 2020: pp. 299 – 309. https://doi.org/10.1007/s11595-020-2257-x
21. **Hu, Y.B., Dong, C.F., Sun, M., Xiao, K., Zhong, P., Li, X.G.** Effects of Solution pH and Cl^- on Electrochemical Behaviour of an Aermet100 Ultra-high Strength Steel in Acidic Environments *Corrosion Science* 53 (12) 2011: pp. 4159 – 4165. https://doi.org/10.1016/j.corsci.2011.08.024
22. **Fan, H.B., Zheng, W., Wang, G.Y., Liaw, P.K., Shen, J.** Corrosion Behavior of Fe41Co7Cr15Mo14C15B6Y2 Bulk Metallic Glass in Sulfuric Acid Solutions *Metallurgical & Materials Transactions Part A* 42 (6) 2011: pp. 1524 – 1533. https://doi.org/10.1007/s11661-010-0500-3